Sensors and Materials, Vol. 37, No. 6 (2025) 2533–2544
MYU Tokyo

S & M 4073

Low-porosity Composite Film of Anodic AlOOH and Thermally Sprayed Y_2O_3 Film for Sensor Application

Chia-Hsien Liu,[1] Hsuan-Jung Chen,[2] Shao-Fu Chang,[3] and Chien-Chon Chen[1,3]*

[1]College of Engineering and Science, Ph.D. Program in Materials and Chemical Engineering,
National United University, No. 2, Lienda, Miaoli 360302, Taiwan
[2]Department of Chemistry, Michigan State University, MI 48824, USA
[3]Department of Energy Engineering, National United University, No. 2, Lienda, Miaoli 360302, Taiwan

(Received February 28, 2025; accepted May 29, 2025)

Keywords: thermal spray, Y_2O_3 coating, anodic film, porosity control, plasma resistance

Low-porosity anodic aluminum oxyhydroxide (AlOOH) composite films and thermally sprayed yttrium oxide (Y_2O_3) films exhibit excellent mechanical strength, chemical corrosion resistance, and high dielectric properties. These characteristics make them promising candidates for applications in the sensor field. Plasma-induced corrosion significantly limits the service life of aluminum components in semiconductor equipment. In this study, we aim to develop a dense, plasma-resistant Y_2O_3 coating on AA6061 substrates through a hybrid approach. A hard anodic oxide layer was first formed to enhance interfacial bonding and buffer thermal stress. Ground Y_2O_3 powder was then applied by thermal spraying to form a 200-μm-thick coating. By reducing the deposition rate, the internal porosity was lowered to approximately 2%. Subsequent aerosol deposition further sealed residual pores, achieving a surface porosity below 0.5%. The resulting composite film exhibited enhanced corrosion resistance, thermal stability, and structural integrity under plasma exposure. This integrated process demonstrates potential for scalable, high-performance protective coatings in advanced semiconductor manufacturing environments.

1. Introduction

In the precision manufacturing industry, key components or devices are manufactured by some manufacturing processes to make structures that continue to be of precise size. Some of these processes are plasma etching and cleaning. Plasma is highly corrosive and may corrode the processing chamber and other surfaces. To increase the lifetime and decrease the particle pollution source from the processing chamber wall, fixture, and accessories, protective coatings are typically deposited on vacuum compounds or chamber walls including a porous body or a pore wall through various methods such as aerosol deposition (AD), thermal spraying, anodization, physical vapor deposition (PVD), ion-assisted deposition, atomic layer deposition (ALD), plasma spraying, and evaporation. Plasma-resistant protective coatings can be deposited via ALD using a precursor such as Al_2O_3, Y_2O_3, ZrO_2, Ta_2O_5, or Er_2O_3.(1–12)

---

*Corresponding author: e-mail: ccchen@nuu.edu.tw
https://doi.org/10.18494/SAM5657

ISSN 0914-4935 © MYU K.K.
https://myukk.org/

The conventional anti-plasma protective film technologies commonly used in semiconductor manufacturing include anodization, thermal spraying, and AD methods. In anodization, a metal surface converts a portion of the metal surface into a metal oxide, thereby creating a metal oxide layer. Anodized metal surfaces provide increased corrosion and wear resistances. Thermal spray coating is performed by heating, melting fine powder, and spraying the molten powder toward the surface to be coated with the base material. The sprayed molten powder is rapidly cooled, solidified, and laminated on the coating target surface mainly by mechanical bonding force. Among thermal spray coating methods, plasma thermal spraying, which uses a high-temperature plasma flame to melt powders, is essential for coating high-melting-point metals, oxides, and ceramics. The thermal spray coating is not only conducive to maintaining the properties of the base material but also produces highly functional materials that exhibit wear resistance, corrosion resistance, heat resistance, high thermal barrier, oxidation resistance, insulation, friction characteristics, heat dissipation, biological function, and radiation resistance.

The AD method is a new technique for depositing ceramic coatings with a wide range of thicknesses, from submicrons to hundreds of microns. The AD method has excellent characteristics, including a high relative plating rate, a high quality of deposited thick films, and low requirements on the process environment. A high-density film is a characteristic of the AD method, in which the density can reach more than 95% and has good plasma resistance. Moreover, the remaining pores in the film are very small, especially compared with those in the sintered bulk sample, with dimensions ranging from 15 to 100 nm. AD films can be prepared at room temperature without any heat treatment. Then, the low vacuum conditions are sufficient for successful AD coating, thereby reducing the workload and cost of process equipment. AD can adapt to a wide range of substrate materials, including metals, glass, ceramics, silicon, polymers, non-oxide materials (TiN, AlN, MgB_2, and MoSi/SiC), and oxide materials (TiO_2, ZrO_2, Y_2O_3, PbO_3, ZrO_3, and TiO_3).(13–17)

The equipment used in the AD method is mainly divided into several components: an aerosol generator, a nozzle with gas supply lines, a mobile platform, and a vacuum chamber. Gas from a high-pressure cylinder passes through a mass flow controller and enters the aerosol generator. In the generator, mechanical vibration suspends a large number of fine particles in the airflow. This particle-laden airflow is then directed to the nozzle, which accelerates the particles to high velocities and propels them toward the substrate. Upon impact, some of the particles adhere to the substrate surface, forming a coating layer. The vacuum chamber is connected to the vacuum pump to maintain a stable back pressure. The substrate is mounted on a mobile platform, which moves the substrate in coordination with the nozzle to deposit a film with the desired shape and thickness.

Many factors affect the velocity of aerosol particles. Among them, the most important factors are the nozzle design and particle size. Another key factor that affects the coating results is whether the aerosol particles are agglomerated. When the aerosol particles are in a state of agglomeration and impacting the substrate, the agglomerated large particles may directly adhere to the substrate, resulting in a large number of pores in the formed coating, affecting the quality of the film. Therefore, the design is extremely important for the aerosol generator.

Y_2O_3 exhibits excellent thermal properties, making it suitable for surface protection layers in semiconductor devices. Under normal circumstances, the Y_2O_3 powder requires hot isostatic pressing and sintering at a temperature exceeding 1700 ℃ to obtain a dense Y_2O_3 bulk. Thermal spraying is a commonly used ceramic coating method across various industries, including semiconductors. However, its main drawback is the high porosity of the sprayed film when there is a mismatch in the thermal expansion coefficients between the coating material and the substrate. As a result, in high-end semiconductor processes, thermal spraying is no longer used as a standalone technique. AD enables the fabrication of highly dense, microscale-thick ceramic films at room temperature within a short period. By AD, high-density coatings (greater than 90%, approaching 100%) can be directly produced from raw ceramic powders, opening new avenues for ceramic coating applications. Moreover, these dense films are typically nanocrystalline, which imparts novel material properties. In general, this method forms thin films dozens of times faster than traditional coating techniques. Then, the porosity of the resulting high-density films can be reduced to below 1%.

Despite advancements in individual coating technologies, there remains a lack of integrated approaches that address both the porosity and interfacial adhesion challenges in Y_2O_3 coatings for plasma environments. In this study, we aim to bridge this gap by combining anodic treatment, thermal spraying, and AD into a single hybrid coating strategy. The goal is to fabricate a Y_2O_3 composite coating with reduced porosity, improved interfacial bonding, and enhanced durability under plasma exposure conditions. Such a coating system holds great potential for extending the service life and performance stability of critical components in semiconductor manufacturing equipment.

In this study, commercial Y_2O_3 powder was ground using a ball milling process for subsequent AD and thermal spraying. The surface morphology of Y_2O_3 films deposited on AA6061 substrates was analyzed by SEM and optical microscopy (OM). The composition was analyzed by elemental dispersion spectroscopy (EDS).

2. Experimental Methods

Hard-film anodization is a specialized anodization process in which the oxide layer exceeds 50 µm in thickness. However, when the thickness surpasses the typical limit, the anodized surface tends to become rough owing to the outward growth of the film. As a result, workpieces such as AA6061 treated with hard anodic films often require secondary mechanical processing or grinding to remove approximately 10 µm of the surface layer. After this post-treatment, the anodized film typically exhibits increased hardness and improved lubricity compared with its pre-polished state.

2.1 Common anodization processes

The common anodization process steps of hard-film anodization include (a) softening (sulfuric acid, 50 ℃), (b) stripping (sodium hydroxide, 75 ℃), (c) chemical cleaning (nitric acid, 25 ℃), (d) chemical polishing (phosphoric acid, 95 ℃), (e) homogenized chemical polishing (ammonium fluoride, 25 °C), (f) anodization (sulfuric acid, −4 °C), (d) de-acidification (clean water, 60 °C), (g) sealing (clean water, 100 °C), and (h) drying (hot air, 50 °C).

2.2 Hard-film anodic treatment

The hard-film anodization treatment in this study simplifies the above steps. The main steps include the following: (1) placing the surface-polished AA6061 sample in an anodization bath containing a mixed acid solution of sulfuric acid + oxalic acid + ethylene glycol (6 vol.% H_2SO_4 + 2.4 wt.% C_2H_2OH + 5 vol.% EG) and under anodization conditions of 1–10 A/cm^2, 70 V, −4 °C, and 0.5–2 h, (2) moving the AA6061 sample out of the anodization bath and into a de-acidification bath (H_2O, 60 °C, 5 min), (3) sealing (H_2O, 100 °C, 40 min), and (4) polishing (1 µm alumina polishing powder) as shown Fig. 1.

2.3 Grinding Y_2O_3 powder

Commercial Y_2O_3 powder with an initial particle size of 2–20 µm was ground to 0.2–2 µm by ball milling. In this experiment, the ball mill was loaded with 3 mm zirconia grinding media and operated using a planetary ball mill for a total grinding time of 3 h. To prevent powder sintering due to excessive heat during milling, the grinding was performed at 30 min intervals with 5 min pauses in between, allowing the Y_2O_3 particles to gradually fracture.

2.4 Measuring equipment

The surface morphology of Y_2O_3 films deposited on AA6061 substrates was analyzed by SEM and OM. The composition was analyzed by EDS.

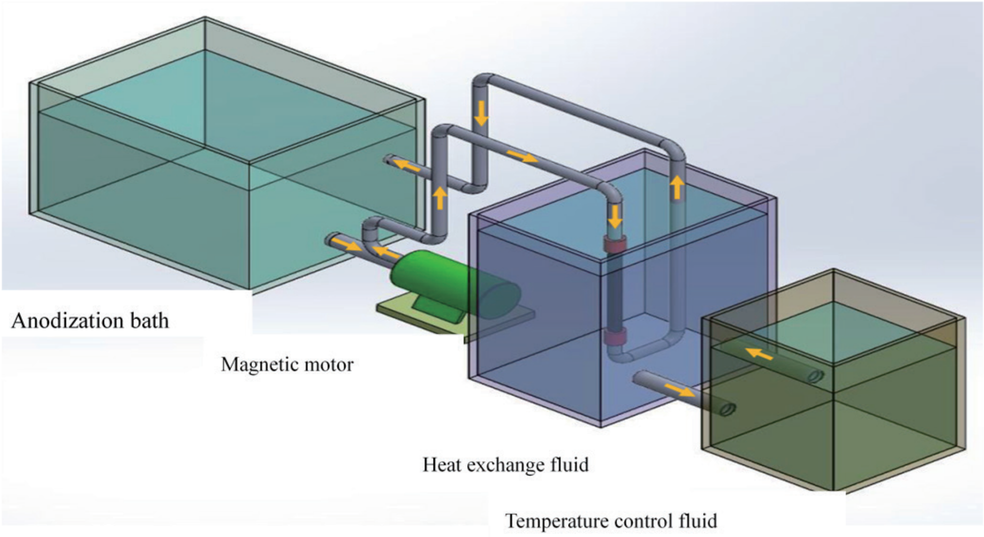

Fig. 1. (Color online) Schematic diagram of anodization bath.

3. Experimental Results

3.1 Y_2O_3 powder morphology analysis after grinding

Figure 2 shows the surface morphology of the Y_2O_3 powder. The commercial Y_2O_3 powder was successfully broken into smaller fragments after ball milling, with the sizes reduced to below 2 µm. EDS analysis confirmed that the composition of Y_2O_3 remained unchanged after milling. When the grinding time was extended for 10 h, the Y_2O_3 powder formed a nearly spherical structure. The size of the particles ranged from 0.1 to 0.2 µm. The EDS elemental analysis showed a consistent Y:O molar ratio of 2:3 as shown in Fig. 3.

Proper powder selection is essential for the successful deposition of oxide films. Powder characteristics affect every stage of the process—from powder delivery and particle acceleration in the nozzle to impact, film build-up, and adhesion. Currently, only general guidelines exist, such as requiring particle sizes in the submicron to micron range. However, the average particle

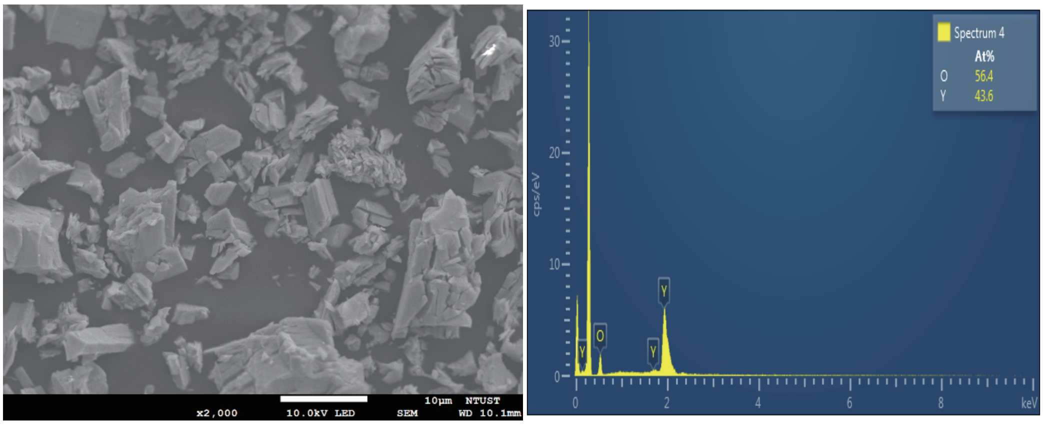

Spectrum 4	At%
O	56.4
Y	43.6

(a) (b)

Fig. 2. (Color online) (a) Microscopy images of fragment shape morphology and (b) EDS composition analysis of Y_2O_3 powder.

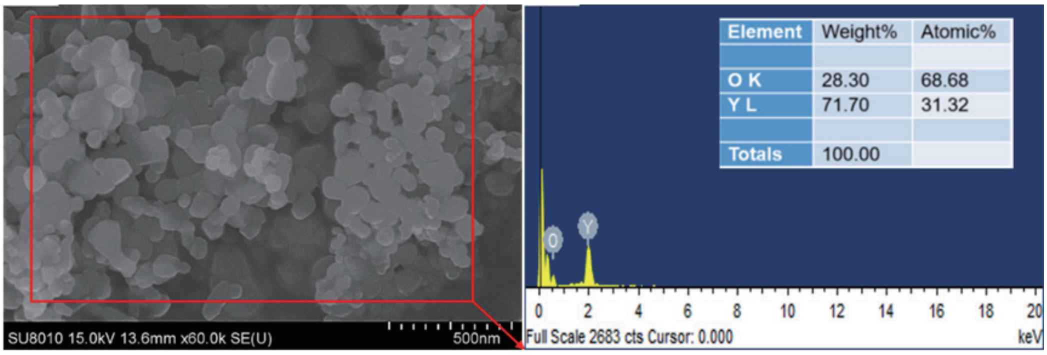

Element	Weight%	Atomic%
O K	28.30	68.68
Y L	71.70	31.32
Totals	100.00	

(a) (b)

Fig. 3. (Color online) (a) Microscopy images of spherical morphology and (b) EDS composition analysis of Y_2O_3 powder.

size alone is insufficient, as factors such as agglomeration, particle porosity, surface roughness, specific surface area, and interparticle friction significantly affect deposition performance. Therefore, establishing a comprehensive set of powder quality assessments is crucial for improving film quality. AD-treated films are characterized by low porosity and the ability to be processed at room temperature. However, they are generally limited by small film thickness and low deposition rate. Typically, AD films serve as secondary layers to reinforce thermally sprayed coatings or anodized layers that serve as the primary thick films. The surface properties of the AD-treated layer enhance the corrosion resistance, particle adhesion stability, and wear resistance of the underlying thick film. Therefore, the properties of the substrate (primary coating) significantly affect the quality of the subsequently deposited AD film. The thermally sprayed film was prepared using ground Y_2O_3 powder. Its microstructural characteristics, porosity, and corrosion resistance are discussed in the following sections.

3.2 AA6061 anodic treatment and mechanism

To enhance the adhesion of thermal spray coatings, a good anti-plasma aluminum component should first be fabricated with an anodic layer on the AA6061 substrate. The common materials used for the anti-plasma layer include Y_2O_3, YAZ, YOF, and YF_3, which are typically deposited onto the anodized surface via thermal spray coating methods. To further suppress the plasma-induced etching of the thermal spray layer, a high-density sealing layer—such as a Y_2O_3 film—can be deposited using a technique such as PVD, ALD, or AD.

First, the anodization steps of the AA6061 substrate are as follows:
(1) stress relief through annealing (200 °C, 30 min),
(2) surface roughness homogenization through surface grinding (#240–2000 SiC sandpaper),
(3) anodization (0 °C, 70 V),
(4) acid regurgitation (deionized water, 25 °C, 5 min), and
(5) boiling water sealing (deionized water, 100 °C, 30 min).

The main reaction formula of aluminum during the anodic treatment process is $Al^{3+} + 3OH^- \rightarrow Al(OH)_3$ and the secondary reaction formula includes $2Al^{3+} + 3H_2O \rightarrow Al_2O_3 + 6H^+$. This secondary reaction generates hydrogen ions. Subsequently, these hydrogen ions can be reduced by electrons arriving at localized cathodic sites (e.g., impurities or conductive regions) via the reaction $2H^+ + 2e^- \rightarrow H_2$. The produced hydrogen escapes from within the anodic film [$Al(OH)_3$], leading to the formation of a tubular structure in the anodic layer.

Figure 4 presents a sequence of process images related to the anodization of AA6061, including (a) a commercial AA6061 sheet, (b) an AA6061 standard sample with a diameter of 10 cm, (c) mechanical grinding, (d) mechanical polishing, (e) anodization, and (f) acid regurgitation, sealing, and final mechanical polishing. The anodization process was carried out under a current density of 5–20 ASD and a final voltage of 30–70 V. Figure 5 presents a series of images showing the anodic film thickness of AA6061 under various anodization conditions. The corresponding current density, anodic voltage, and resulting film thickness for each condition are also summarized in the figure. The main reaction formula of aluminum anodization is $Al^{3+} + 3OH^- \rightarrow Al(OH)_3$. According to Faraday's laws, the relationship between the anodization current and the film thickness can be expressed as Eqs. (1) and (2).

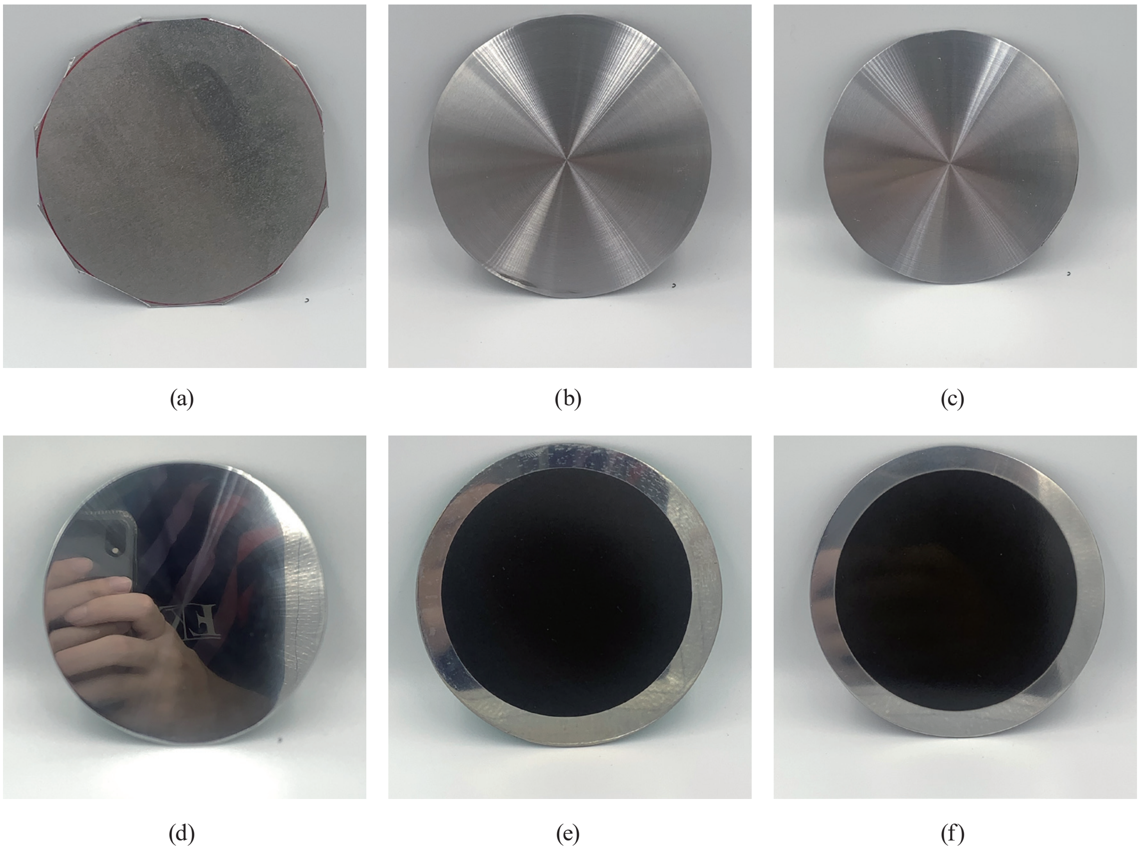
(a) (b) (c)
(d) (e) (f)

Fig. 4. (Color online) Images of AA6061 anodization process. (a) Commercial AA6061 sheet. (b) AA6061 with a standard sample of 10 cm diameter. (c) After mechanical grinding. (d) After mechanical polishing. (e) After anodization. (f) After mechanical polishing.

$$Q = I \times t = n \times F \times N = \frac{n \times F \times \rho \times D \times A}{M} \tag{1}$$

$$D = \frac{I \times t \times M}{n \times F \times \rho \times A} \tag{2}$$

Here, Q is charge (C), I is current (A), T is time (s), n is dissociation valence, F is Faraday constant (96500), N is mole number (mole), ρ is density (g/cm^3), D is thickness (cm), A is area (cm^2), and M is molecular weight (g/mol).

3.3 Porosity analysis of Y_2O_3 films after anodic treatment and thermal spraying

Figure 6 shows a photograph of a larger area of AA6061 after the anodization and thermal spraying of Y_2O_3 films. Figure 6(a) shows the uniform formation of a black film on AA6061. Figure 6(b) shows the white Y_2O_3 film thermally sprayed on the anodic film. There is

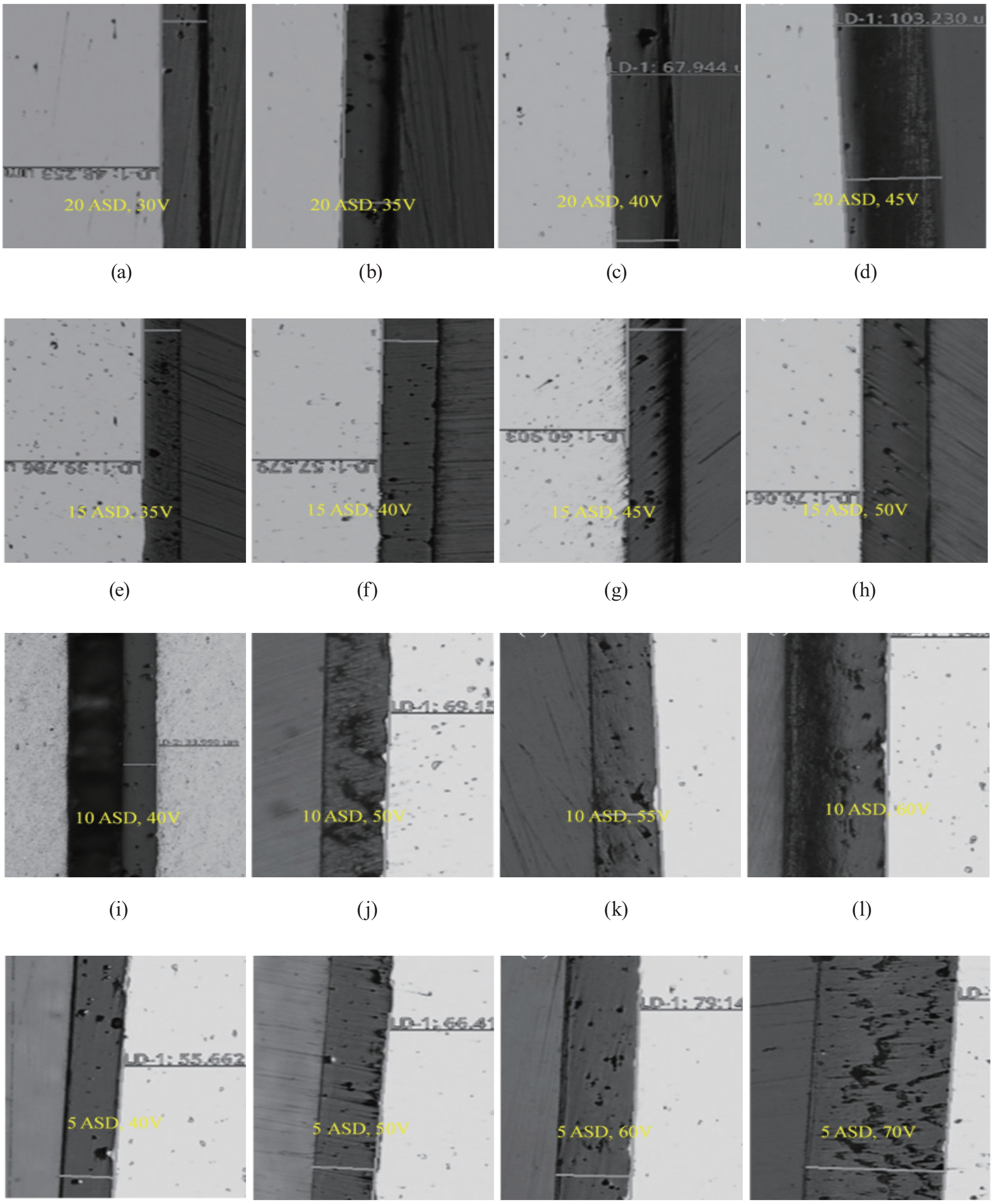

(a) (b) (c) (d)

(e) (f) (g) (h)

(i) (j) (k) (l)

(m) (n) (o) (p)

Fig. 5. (Color online) Microscopy images showing AA6061 anodic film thickness under various currents and applied voltages. (a) 48, (b) 60, (c) 68, (d) 103, (e) 40, (f) 58, (g) 61, (h) 70, (i) 33, (j) 69, (k) 70, (l) 108, (m) 55, (n) 66, (o) 79, and (p) 146 μm.

considerable demand for minimal anodization in the surface treatment of semiconductor equipment. Semiconductor equipment, such as vacuum aluminum chamber components, can

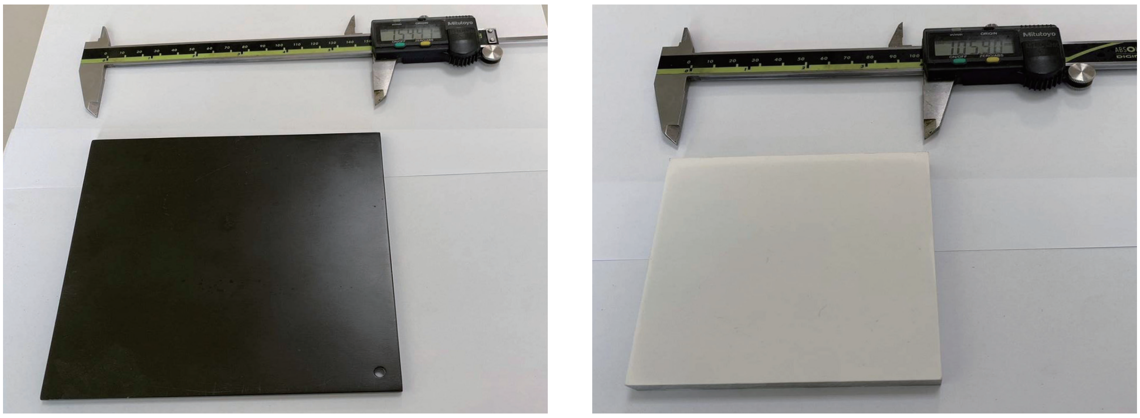

(a) (b)

Fig. 6. (Color online) Images of (a) anodic and (b) thermally sprayed Y_2O_3 films on AA6061 surface.

react with plasma halogen-containing gas to form aluminum chloride and aluminum fluoride by chemical methods. The thick part of the components may be peeled off and contaminated by corrosion, leading to a decrease in wafer yield. The corrosion resistance of a chamber component must be improved by forming a coating of corrosion-resistant material on the surface of an overly susceptible component, such as a surface that is exposed to an excited gas, which must be frequently replaced or removed from the chamber and cleaned, resulting in undesirable chamber downtime. The corrosion resistance coating layer can be improved by a composite film with anodization and thermal spraying coating, especially in dry etching environments. However, while such coatings improve the corrosion resistance of chamber components, the sprayed layer may also create other problems, such as thermal expansion mismatch between the coating and the underlying component structure causing the coating to peel off from the underlying structure, thereby exposing the corrosive nature of the substrate, or loose particles of coating material break off and contaminate the chamber. In our study, the anodic film serves as a thermal expansion buffer layer at the interface between Y_2O_3 and AA6061. Its primary function is to reduce the peeling of the Y_2O_3 coating in high-temperature plasma environments.

Figure 7 shows the vertical OM image (side view) of the thermally sprayed Y_2O_3 film on the surface of the aluminum substrate [magnifications of (a) ×50, (b) ×100, (c) ×200, and (d) ×500]. The result shows that local holes are formed inside the thermally sprayed Y_2O_3 film, with a porosity of about 5–10%, including larger holes. Figure 8 shows a more detailed vertical OM image of the thermally sprayed Y_2O_3 film on the surface of the aluminum substrate. The surface of the aluminum substrate has been sandblasted to obtain greater roughness and improve the adhesion of the Y_2O_3 film on the surface of the aluminum substrate. The thickness of the Y_2O_3 film is 200 μm and its surface roughness is about Ra 2 μm. Local holes are formed inside the Y_2O_3 film. The porosity is about 7–10% as shown in Fig. 8. Decreasing the deposition rate of the thermally sprayed Y_2O_3 film during thermal spraying (increased process costs) can reduce the porosity of the thermally sprayed Y_2O_3 film.

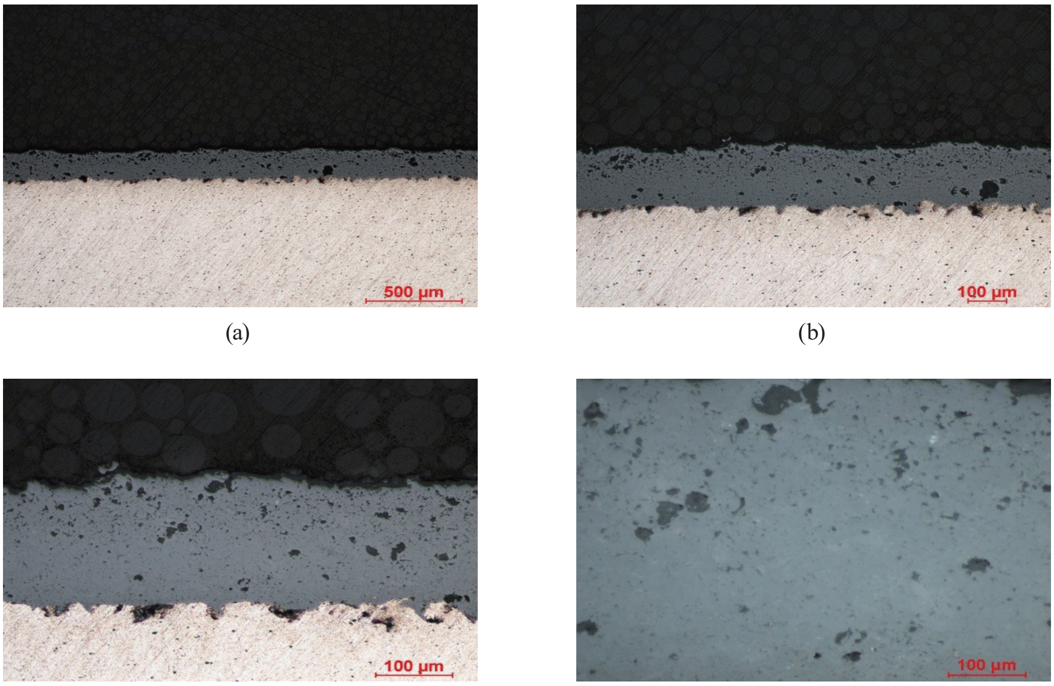

(a) (b)

(c) (d)

Fig. 7. (Color online) OM image (side view) of thermally sprayed Y_2O_3 film on AA6061 surface.

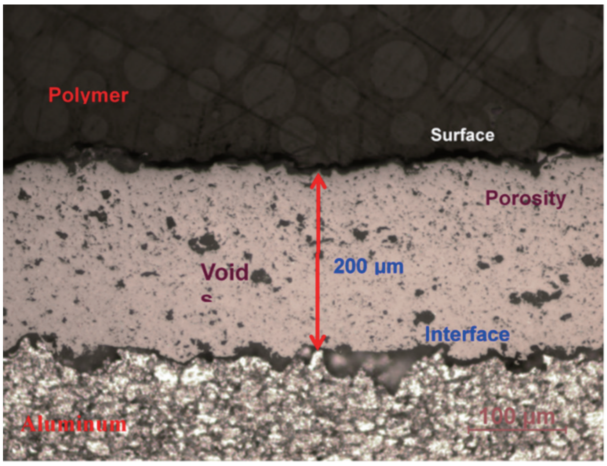

Fig. 8. (Color online) OM image (side view) of Y_2O_3 film thermally sprayed on AA6061 surface.

Figure 9 shows that by applying low thermal spray deposition, a 200-µm-thick Y_2O_3 layer was formed on the surface of an aluminum substrate. The image analysis revealed that the surface porosity of the film was reduced to approximately 2%. Owing to this lower initial porosity, subsequent AD can further fill the remaining pores, reducing the surface porosity to below 0.5%. This low-porosity Y_2O_3 film is expected to be applied as a protective coating on the surfaces of next-generation semiconductor vacuum chambers, where increasingly stringent plasma resistance is required. These characteristics make them promising candidates for applications in the sensor field.

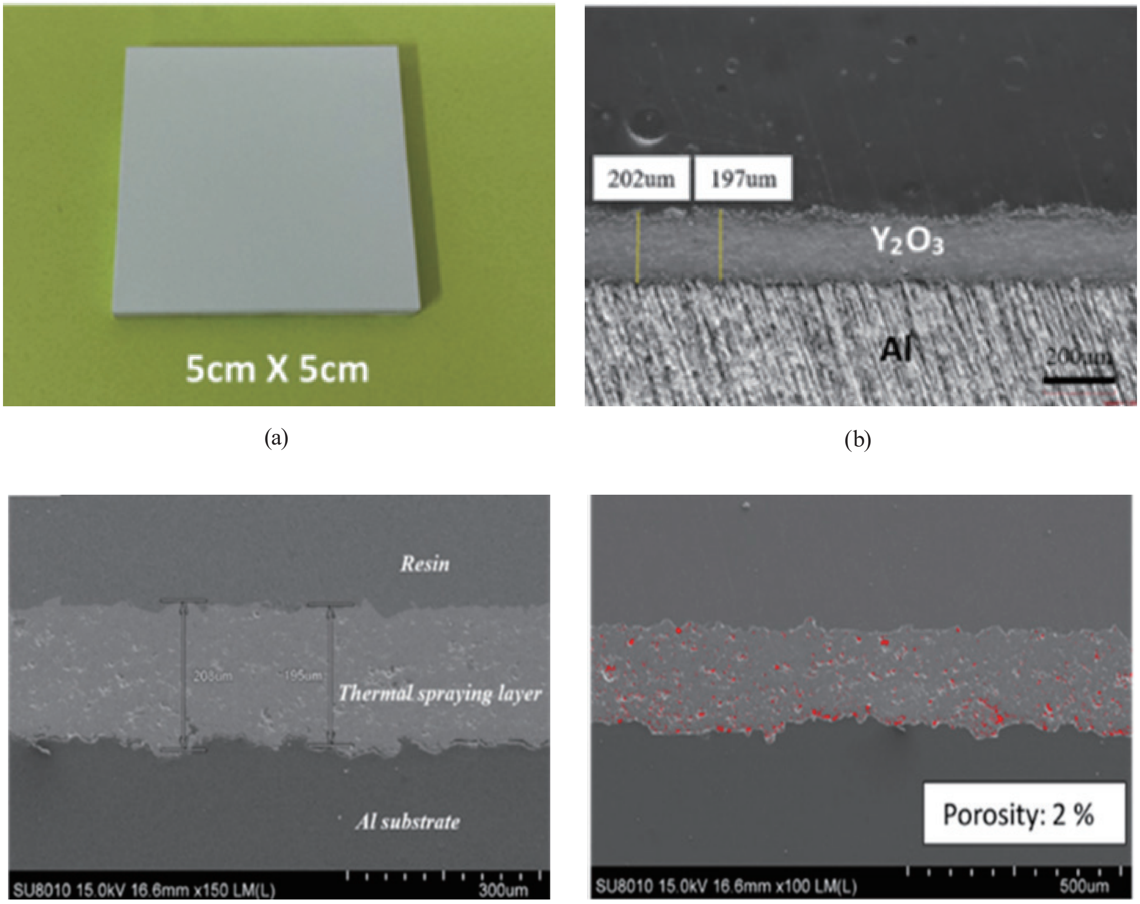

(a) (b)

(c) (d)

Fig. 9. (Color online) (a) Physical image of Y_2O_3 powder thermally sprayed on aluminum substrate. (b) The thickness of the thermal spray coating is 200 μm (observed by OM). (c) The thickness of the thermal spray coating is 200 μm (observed by SEM). (d) The porosity of the thermal spray coating is approximately 2%.

4. Conclusions

In this study, we investigated a low-porosity, composite Y_2O_3 coating system designed for anti-plasma applications in semiconductor environments. The fabrication process involved three key steps: the anodization of the AA6061 aluminum substrate to improve interfacial bonding and thermal stability, the thermal spraying of ground Y_2O_3 powder to form a thick protective layer, and AD to densify the surface and reduce porosity. The experimental results demonstrate that anodizing the aluminum substrate successfully forms an AlOOH interlayer, which significantly improves adhesion and provides a thermal expansion buffer between the aluminum base and the ceramic coating. Following this, the thermal spraying of ground Y_2O_3 powder produced a 200-μm-thick protective layer, but with an initial internal porosity of 7–10%. By adjusting the spraying parameters and reducing the deposition rate, the porosity was effectively lowered to approximately 2%. Subsequently, AD further sealed the residual pores, resulting in a final surface porosity of less than 0.5%. This composite coating structure showed marked improvements in durability, thermal stability, and plasma resistance. Overall, the proposed hybrid process demonstrates high potential as a scalable, cost-effective method for fabricating anti-plasma coatings suitable for demanding applications in the semiconductor, aerospace, and defense industries.

Acknowledgments

This work was financially supported by 2024 Chung-Shan Institute of Science and Technology [NCSIST-1847-V302(114)] and 2024 National Science and Technology Council, R.O.C. (113-2218-E-002 -026 -).

References

1 S. H. Liu, J. P. Trelles, C. J. Li, C. X. Li, and H. B. Guo: Mater. Today Phys. **27** (2022) 100832. https://doi.org/10.1016/j.mtphys.2022.100832

2 Y. C. Cao, L. Zhao, J. Luo, K. Wang, B. P. Zhang, H. Yokota, Y. Ito, and J. F. Li: Appl. Surf. Sci. **366** (2016) 304. https://doi.org/10.1016/j.apsusc.2016.01.092

3 Y. H. Zhang, Y. N. Sun, X. Tan, C. Wang, S. J. Li, C. M. Deng, Y. F. Xu, and S. P. Niu: Surf. Coat. Technol. **459** (2023) 129405. https://doi.org/10.1016/j.surfcoat.2023.129405

4 C. Jiang, X. Ji, Y. X. Chen, P. P. Wang, P. V. Kiryukhantsev-Korneev, E. A. Levashov, J. Shi, X. R. Ren, X. Q. Kang, B. J. Zhang, P. Zhang, L. H. Xu, and P. Z. Feng: J. Eur. Ceram. Soc. **45** (2025) 117293. https://doi.org/10.1016/j.jeurceramsoc.2025.117293

5 Z. G. Wang, J. E. Liu, S. Han, B. C. Liu, J. D. Wang, S. X. Zeng, C. X. Wang, S. Y. Min, Y. Y. Hu, P. Bo, Q. Wang, H. Y. Li, D. Z. Liu, P. Wen, Y. F. Zheng, and Y. Tian: Adv. Funct. Mater. **35** (2025) 18. https://doi.org/10.1002/adfm.202414264

6 S. Lee, H. Kim, and S. Kwon: Coatings **15** (2025) 22. https://doi.org/10.3390/coatings15010022

7 E. K. Park, H. Y. Jang, S. Y. Jeon, K. Raju, and H. K. Lee: Materials **17** (2024) 4585. https://doi.org/10.3390/ma17184585

8 Y. L. Chu, S. J. Young, S. H. Tsai, S. Arya, and T. T. Chu: ACS Appl. Electron. Mater. **6** (2024) 712. https://doi.org/10.1021/acsaelm.3c01138

9 X. R. Dong, D. W. Wang, H. L. Jia, K. Zhang, Y. Z. Chen, Y. J. Yang, and M. Zha: Corros. Sci. **236** (2024) 112230. https://doi.org/10.1016/j.corsci.2024.112230

10 S. Inoue, K. Iwanaga, and Y. Kawamura: J. Magnesium Alloys **12** (2024) 742. https://doi.org/10.1016/j.jma.2024.01.017

11 Q. Y. Song, Y. Li, H. Kimura, G. G. Wang, S. Z. Zhang, J. Guo, W. W. Wang, S. X. Du, Z. H. Li, J. X. Qiu, and P. Ren: Surf. Coat. Technol. **477** (2024) 130315. https://doi.org/10.1016/j.surfcoat.2023.130315

12 J. S. Wang, X. J. Lu, C. X. Shu, Z. X. Duan, S. J. Dong, G. Q. Lu, Y. X. Zhang, F. H. Yuan, and X. Q. Cao: Ceram. Int. **50** (2024) 5111. https://doi.org/10.1016/j.ceramint.2023.11.255

13 Y. L. Chu, S. J. Young, Y. R. Huang, S. Arya, and T. T. Chu: ACS Appl. Electron. Mater. **7** (2025) 129. https://doi.org/10.1016/j.jallcom.2025.179255

14 S. H. Chen, S. J. Young, C. C. Yang, and Y. H. Liu: J. Mater. Sci.: Mater. Electron. **36** (2025) 478. https://doi.org/10.1007/s10854-025-14436-4

15 Y. H. Liu, S. J. Young, L. W. Ji, Y. L. Chu, and S. J. Chang: Talanta Open **10** (2024) 100386. https://doi.org/10.1016/j.talo.2024.100386

16 S. J. Young, Y. J. Chu, and Y. H. Liu: IEEE Sens. J. **24** (2024) 36664. https://doi.org/10.1109/JSEN.2024.3466185

17 C. H. Wang, H. X. Zhou, S. H. Liu, C. X. Li, and C. J. Li: Surf. Coat. Technol. **494** (2024) 131261. https://doi.org/10.1016/j.surfcoat.2024.131261